Developmental Cell
Article

MeCP2 Suppresses Nuclear MicroRNA Processing and Dendritic Growth by Regulating the DGCR8/Drosha Complex

Tian-Lin Cheng,[1,4] Zhizhi Wang,[2] Qiuming Liao,[1] Ying Zhu,[1] Wen-Hao Zhou,[3] Wenqing Xu,[2] and Zilong Qiu[1,*]
[1]Institute of Neuroscience, Shanghai Institutes for Biological Sciences, Chinese Academy of Sciences, Shanghai 200031, China
[2]Department of Biological Structure, University of Washington, Seattle, WA 98195, USA
[3]Department of Neonatology, Children's Hospital, Fudan University, Shanghai 201102, China
[4]University of Chinese Academy of Sciences, Beijing 100049, China
*Correspondence: zqiu@ion.ac.cn
http://dx.doi.org/10.1016/j.devcel.2014.01.032

SUMMARY

Loss- and gain-of-function mutations of the X-linked gene *MECP2* (methyl-CpG binding protein 2) lead to severe neurodevelopmental disorders in humans, such as Rett syndrome (RTT) and autism. MeCP2 is previously known as a transcriptional repressor by binding to methylated DNA and recruiting histone deacetylase complex (HDAC). Here, we report that MeCP2 regulates gene expression posttranscriptionally by suppressing nuclear microRNA processing. We found that MeCP2 binds directly to DiGeorge syndrome critical region 8 (DGCR8), a critical component of the nuclear microRNA-processing machinery, and interferes with the assembly of Drosha and DGCR8 complex. Protein targets of MeCP2-suppressed microRNAs include CREB, LIMK1, and Pumilio2, which play critical roles in neural development. Gain of function of MeCP2 strongly inhibits dendritic and spine growth, which depends on the interaction of MeCP2 and DGCR8. Thus, control of microRNA processing via direct interaction with DGCR8 represents a mechanism for MeCP2 regulation of gene expression and neural development.

INTRODUCTION

Loss-of-function mutations in methyl-CpG binding protein 2 (*MECP2*) gene are primary causes for Rett syndrome (RTT) (Amir et al., 1999; reviewed in Chahrour and Zoghbi, 2007), whereas the duplications of *MECP2*-containing loci may lead to autism spectrum disorders in human (Ramocki et al., 2009). Therefore, the dose of MeCP2 protein is critical for the proper development and function of the central nervous system (CNS). MeCP2 was found to primarily bind to methylated CpG islands and acts as a transcriptional repressor by recruiting histone deacetylase complex (HDAC) (Lewis et al., 1992; Nan et al., 1993, 1998; reviewed in Guy et al., 2011). MeCP2 has been shown to play critical roles in regulating gene expression transcriptionally, including brain-derived neurotrophic factor (BDNF) and other genes important for the proper function of the CNS (Chen et al., 2003; Martinowich et al., 2003; Tao et al., 2009; Zhou et al., 2006). Furthermore, MeCP2 was found to regulate synaptic homeostasis by transcriptionally repressing GluA2 expression in an activity-dependent manner (Qiu et al., 2012). Posttranslational modifications of MeCP2 play critical roles in regulating neural development (Cohen et al., 2011). For example, the activity-dependent phosphorylation of Serine 421 (Ser421) of MeCP2 is critical for regulating the recruitment of MeCP2 on DNA and expression of target genes such as BDNF (Cohen et al., 2011; Zhou et al., 2006), and the interaction between MeCP2 and the nuclear receptor corepressor complex (NCoR) is regulated by an activity-dependent phosphorylation of Thr308 of MeCP2 (Ebert et al., 2013; Lyst et al., 2013).

Transcriptome-wide studies revealed that expression of many genes is repressed in the brain of *mecp2* null mice, suggesting a positive role for MeCP2 in gene regulation (Chahrour et al., 2008). An alternative possibility is that MeCP2 controls posttranscriptional regulators, e.g., microRNAs (miRNAs), which are known to specifically suppress generation of many proteins that are important for cell proliferation, development, and tumorigenesis (Bartel, 2004; Bushati and Cohen, 2007; Fire et al., 1998). The biogenesis of miRNAs begins with the transcription of the primary miRNAs from the genome, followed by its processing through Drosha/DiGeorge syndrome critical region 8 (DGCR8)-containing nuclear machinery and cytosolic Dicer complex (Denli et al., 2004; Gregory et al., 2004; Han et al., 2004; Lee et al., 2003). It was reported recently that miRNA expression profile was altered in the brain of *mecp2* null mouse due to the transcriptional repression function of MeCP2 (Szulwach et al., 2010; Urdinguio et al., 2010; Wu et al., 2010). Whether MeCP2 may participate in the miRNA processing directly other than the transcription process is unknown.

In this study, we found that MeCP2 regulates gene expression posttranscriptionally by regulating nuclear miRNA processing directly. We showed that MeCP2 directly interacts with DGCR8, a critical component of the nuclear miRNA-processing complex, through its C-terminal domain. The phosphorylation of Ser80 of MeCP2 is crucial for binding to DGCR8, which is rapidly dephosphorylated by neuronal calcium signaling. Interestingly, the phosphorylation of Ser80 regulates an intramolecular interaction switch of MeCP2, which leads to an "open" form of the MeCP2 protein and facilitates its binding with DGCR8. We

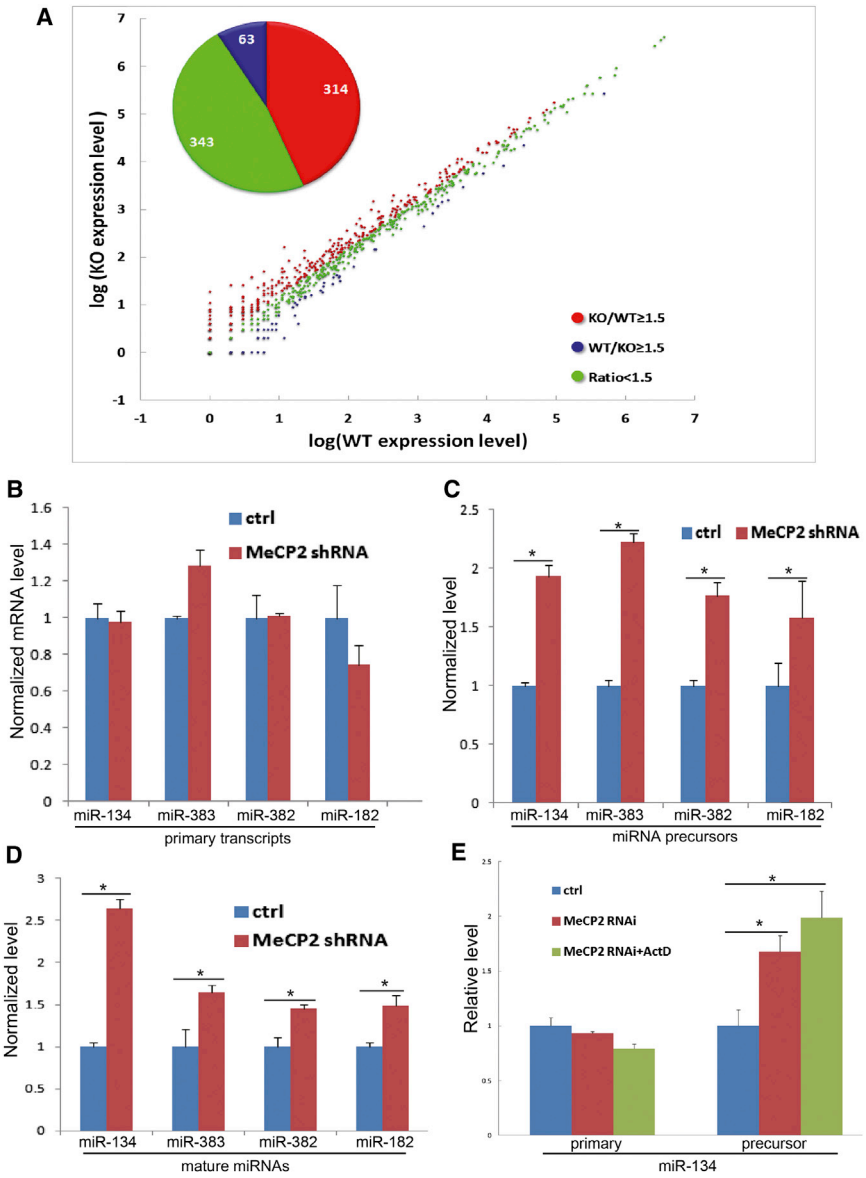

Figure 1. Upregulation of Mature miRNAs in the Hippocampus of *mecp2* Null Mice and the Role of MeCP2 in miRNA Processing

(A) Deep-sequencing data on the level of 720 mature miRNAs in hippocampal tissues from WT and *mecp2* null (KO) mice. A total of 314 showed higher expression by ≥1.5-fold (red circles), and 63 showed ≤1.5-fold lower expression (blue circles) in KO mice, as compared to WT mice. The rest showed differences in expression level <1.5-fold (green circles). The pie chart depicts the percentage of three populations.

(B–D) Examination of primary, precursor, and mature miR-134, miR-383, miR-382, and miR-182 levels in MeCP2-shRNA-expressing neuron lysates. Lentivirus-harboring MeCP2 RNAi was seeded to mouse primary cortical neurons 2 DIV, and RNA samples were collected 5 days after viral infection. Primary, precursor, and mature miRNA levels were analyzed with qPCR. ctrl, control samples with GFP expression only.

(E) Examination of primary and precursor miR-134 levels in the presence of transcriptional blocker. Procedures similar to those described in (B) were used. Actinomycin D (1 μM) was applied for 3 hr prior to RNA collection. Primary and precursor miR-134 levels were analyzed with qPCR.

*$p < 0.05$ (t test). See also Figure S1 and Table S1.

further provided evidence showing that MeCP2 controls brain-enriched miR-134 processing and thus regulates three of its downstream target genes: cAMP-responsive element-binding protein (CREB), LIM domain kinase 1 (LIMK1), and Pumilio2. These results demonstrate the role for MeCP2 in participating in nuclear miRNA processing directly and suggest a mechanism for which dysregulation of MeCP2 levels leads to neurodevelopmental disorders.

RESULTS

Upregulation of miRNAs in *mecp2* Null Mice

To determine whether the miRNA expression profile is altered by MeCP2, we performed Solexa-based RNA sequencing (RNA-seq) to assess global changes in the expression pattern of miRNAs caused by the loss of MeCP2 in *mecp2* null (knockout [KO]) mice (Chen et al., 2001). Normalized with total reads, 314 of all 720 (43.6%) sequenced miRNAs from the hippocampus of *mecp2* KO mice were found to be significantly upregulated for over 1.5-fold, as compared to those found in the wild-type (WT) littermates (Figure 1A; Table S1A available online). In contrast, only 63 (8.7%) of them were downregulated. To determine whether overexpression of MeCP2 would inhibit miRNA biogenesis, we applied RNA-seq to mouse cortical neurons with MeCP2 overexpressed by lentiviral-based gene delivery. We found that miRNAs are dramatically repressed: 243 of all 373 (65.1%) decreased expression for 1.5-fold with elevated MeCP2 protein level (Table S1B). Among the upregulated miRNAs in *mecp2* KO and downregulated miRNAs in MeCP2 overexpression, there are 106 miRNAs overlapped (Tables S1A and S1B). These data indicated that MeCP2 significantly regulates miRNA biogenesis.

Among the upregulated miRNAs in the hippocampus of *mecp2* KO mice, we examined the level of 15 primary miRNA transcripts that showed high expression in the CNS and found that 12 of 15 showed no significant changes in the primary transcripts (Figure S1A), suggesting that miRNA upregulation in *mecp2* KO mice is most likely caused by the loss of suppressive action of MeCP2 on miRNA processing. To confirm the role of MeCP2 in miRNA processing, we examined the primary, precursor, and mature level of several candidate miRNAs repressed by MeCP2, including miR-134, miR-383, miR-382, and miR-182. We found that primary transcripts of these miRNAs are not altered in neurons expressing either short hairpin RNA (shRNA)

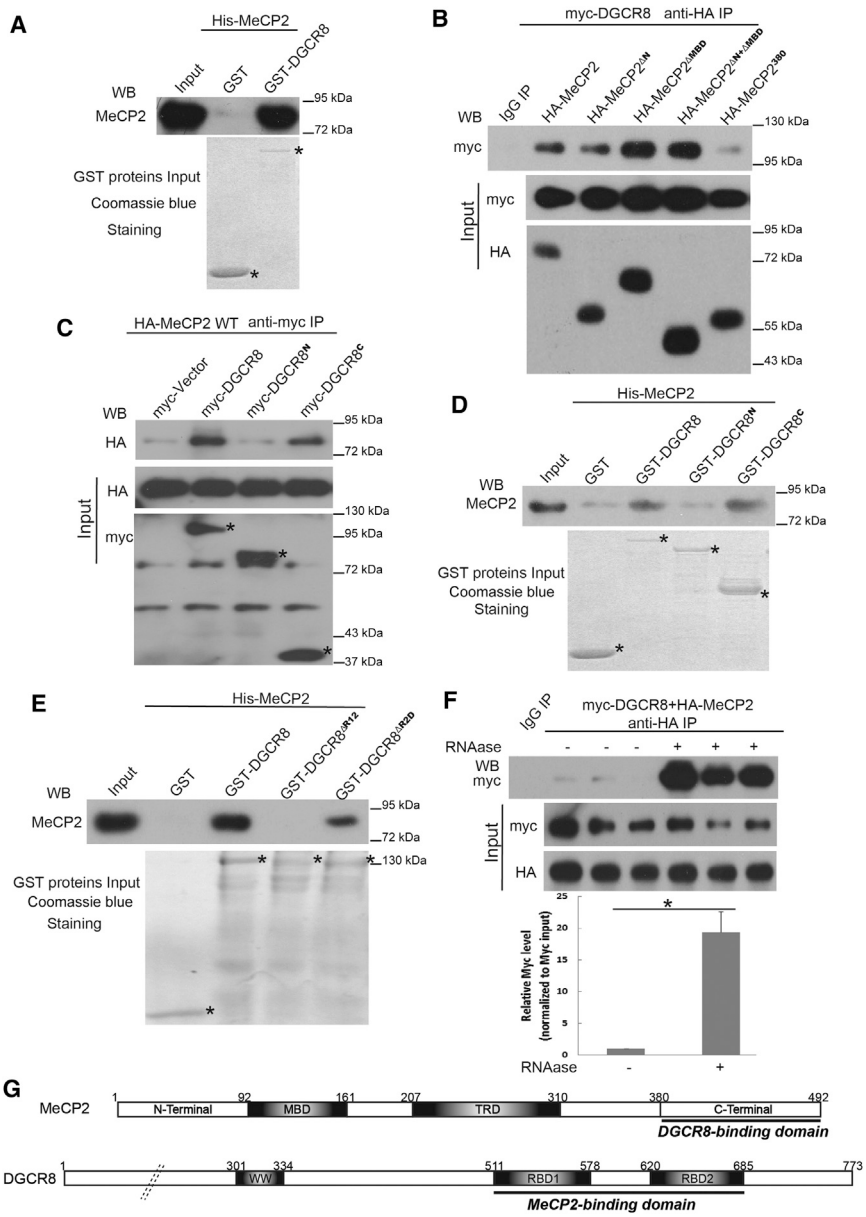

Figure 2. The Direct Interaction between MeCP2 and DGCR8

(A) Direct interaction between MeCP2 and DGCR8 shown by GST pull-down assay. The recombinant GST and GST-DGCR8 purified from bacterial sources were immobilized on glutathione beads, combined with purified His-MeCP2, washed, and analyzed on SDS-PAGE using antibodies indicated. Target bands are indicated by asterisks. WB, western blot.

(B) Interaction between various MeCP2 forms and DGCR8 in HEK293 cells. HA-tagged WT or mutated forms of MeCP2 were coexpressed with myc-tagged DGCR8. Cell lysates were immunoprecipitated with anti-HA antibody and analyzed on SDS-PAGE. MeCP2$^{\Delta N}$, N terminus (aa 1–91) deleted; MeCP2$^{\Delta MBD}$, methyl-DNA-binding domain (aa 92–161) deleted; MeCP2$^{\Delta N+\Delta MBD}$, both N terminus and MBD (aa 1–161) deleted; MeCP2^{380}, C-terminal segment (aa 380–492) deleted. IP, immunoprecipitation.

(C) Interaction between various DGCR8 forms and MeCP2 in 293T cells. Myc-tagged WT, N segment, or C segment of DGCR8 was coexpressed with HA-tagged MeCP2. Cell lysates were immunoprecipitated with anti-myc antibody and analyzed on SDS-PAGE. DGCR8^{N}, (aa 484–773) deleted; DGCR8^{C}, (aa 1–483) deleted.

(D) Direct interaction between MeCP2 and DGCR8^{C} shown by GST pull-down. Procedures similar to those described in (A) were used.

(E) Direct interaction of MeCP2 with both RBD domains of DGCR8. DGCR8$^{\Delta R12}$, (aa 511–685) deleted; DGCR8$^{\Delta R2D}$, (aa 620–750) deleted.

(F) The role of RNA in the interaction of MeCP2 and DGCR8. HA-MeCP2 and myc-DGCR8 were cotransfected into 293T cells. RNase (final concentration of 0.25 μg/μl, 37°C for 30 min) was used to digest RNA prior to immunoprecipitation. Cell lysates were immunoprecipitated with IgG and anti-HA antibody and analyzed on SDS-PAGE. Lower panel shows quantitation of upper panel. Error bars are SEM.

(G) Schematic illustration of interaction domains of MeCP2 and DGCR8.

*$p < 0.05$ (t test). See also Figures S2 and S3.

or small interfering RNA (siRNA) against MeCP2, whereas the precursor and mature levels of these miRNAs are significantly increased (Figures 1B–1D and S1B). We further examined the primary, precursor, and mature levels of miR-134 in neurons overexpressing MeCP2 and found that precursor and mature forms of miR-134 were significantly downregulated by MeCP2 overexpression, but not primary miR-134 (Figure S1C), suggesting that MeCP2 regulates the expression of these miRNAs through a transcription-independent mechanism.

Furthermore, we measured the levels of primary and precursor miR-134, one of MeCP2-repressed miRNAs, in the presence of transcriptional blocker actinomycin D when MeCP2 was knocked down by RNAi. We found that the upregulation of miR-134 precursor by MeCP2 RNAi is not affected by actinomycin D treatment, further confirming that MeCP2 represses miR-134 expression in a transcription-independent manner (Figure 1E).

Direct Interaction of MeCP2 with DGCR8

To understand how MeCP2 regulates miRNA processing, we performed glutathione S-transferase (GST) pull-down assays using bacteria-purified MeCP2 to examine the interaction between MeCP2 and components of the nuclear miRNA-processing complex. We found that there was a direct interaction between MeCP2 and DGCR8 (Figure 2A). Previous works showed that the C terminus of MeCP2 may be critical for the interaction between MeCP2 and RNA-binding proteins (Buschdorf and Strätling, 2004; Young et al., 2005). Frame-shifting and truncated mutations around amino acid 380, which led to a deletion of ~100 aa from the C terminus, are frequently identified mutations

in patients with RTT (Bebbington et al., 2010). The C-terminal deletions accounted for 15% of all genetic mutations identified among the patients with RTT (Bebbington et al., 2010). We found that in lysates of HEK293 cells, the binding of MeCP2^{380} (a MeCP2 mutant with deletion of residues 380–492) with coexpressed DGCR8 was significantly weaker than that of the WT MeCP2 (Figure 2B). In contrast, binding with DGCR8 was not affected for MeCP2$^{\Delta N}$, MeCP2$^{\Delta MBD}$, and MeCP2$^{\Delta N+\Delta MBD}$, which have the N terminus (aa 1–91), methyl-DNA-binding domain (aa 92–161), and both domains deleted, respectively (Nan et al., 1993; Figure 2B). The schematic illustration of domains of MeCP2 and DGCR8 is shown Figures S2A and S2B. Thus, the interaction of MeCP2 with DGCR8 depends on its C terminus, but not the methyl-DNA-binding domain.

To characterize the direct interaction between MeCP2 and DGCR8, we determined the binding affinity between DGCR8 and MeCP2 using Alpha Technology assay. Purified mouse DGCR8^{C} interacted with MeCP2$^{\Delta N+\Delta MBD}$ with an apparent K_d value of 385 nM. This result further confirms the direct interaction between DGCR8 and MeCP2 (Figures S3A and S3B).

Next, we examined whether MeCP2^{380} is still able to act as a transcriptional repressor. We measured the mRNA level of the BDNF gene, a well-known MeCP2 transcriptional target, in mouse primary cortical neurons (Chen et al., 2003). We found that BDNF mRNA is upregulated when MeCP2 is knocked down by RNAi, consistent with previous findings, and both WT MeCP2 and MeCP2^{380} are able to fully rescue BDNF mRNA to a normal level, indicating that MeCP2^{380} retains its transcriptional repressor activity (Figure S4A; Zhou et al., 2006). We further examined the mRNA level of Acta2, a candidate gene repressed by MeCP2, in mouse primary cortical neurons. We found that Acta2 mRNA level was significantly downregulated by expression of either WT or 380 truncated form of MeCP2, indicating that MeCP2^{380} is able to exhibit transcriptional repression activity as WT MeCP2 (Figure S4B).

To further investigate which domain of DGCR8 is responsible for binding to MeCP2, we generated N- and C-terminal halves of DGCR8, consisting of residues 1–483 (DGCR8^{N}) and 484–773 (DGCR8^{C}), respectively (Figure S2B). Coimmunoprecipitation (coIP) studies showed that the interaction with MeCP2 was reduced for DGCR8^{N} but not for DGCR8^{C}, as compared to full-length DGCR8 (Figure 2C). Furthermore, the GST pull-down experiments with purified proteins showed that MeCP2 directly binds to DGCR8^{C}, but not DGCR8^{N} (Figure 2D). Thus, a domain responsible for the interaction with MeCP2 is located in DGCR8^{C}.

Because DGCR8^{C} contains two RNA-binding domains and a C-terminal tail that is required for Drosha binding (Yeom et al., 2006), we prepared mutated forms of DGCR8 with deletions in various domains: DGCR8$^{\Delta R12}$ deleted both RNA-binding domains; and DGCR8$^{\Delta R2D}$, a mutated form, deleted RNA-binding domain 2 and the Drosha-binding C-terminal tail (Figure S2B). We found that DGCR8$^{\Delta R12}$ has no interaction with MeCP2, but deletion of either one of the RNA-binding domains or Drosha-binding domain had no effect (Figures 2E and S4C).

Because RNA-binding domains of DGCR8 are involved in MeCP2 interaction, we also examined whether the presence of RNA is critical for interaction of MeCP2 and DGCR8. We performed an immunoprecipitation experiment with and without ribonuclease (RNase) treatment. Surprisingly, we found that the interaction between MeCP2 and DGCR8 became much stronger when RNAs were digested by RNase, suggesting that MeCP2 may play a negative role in regulating the association of DGCR8 with its RNA substrates (Figure 2F).

These results indicate that both RNA-binding domains of DGCR8 are responsible for directly binding to MeCP2. Interaction domains of MeCP2 and DGCR8 are illustrated in Figure 2G.

MeCP2 Competes with Drosha for Binding to DGCR8 and RNA

To explore the mechanism by which MeCP2 regulates nuclear miRNA processing, we tested the possibility that the interaction between MeCP2 and DGCR8 interferes with DGCR8 binding to Drosha, which is the essential RNase III enzyme interacting with the C terminus of DGCR8 in the miRNA-processing complex (Yeom et al., 2006). First, we confirmed by coIP experiments that, in HEK293 cells overexpressing full-length DGCR8, DGCR8^{N}, or DGCR8^{C}, only DGCR8 and DGCR8^{C} bind to endogenous Drosha (Figure 3A). Next, we tested the effect of MeCP2 on the binding of DRCR8 with Drosha. We coexpressed DGCR8 with either full-length MeCP2 or MeCP2^{380} in HEK293 cells, and coIP results showed that the binding of DGCR8 with Drosha was significantly weaker in the presence of the full-length MeCP2, but not MeCP2^{380} (Figure 3B). We further confirmed this finding by examining the interaction between DGCR8 and Drosha in the presence of MeCP2 in a dose-dependent manner. We coexpressed DGCR8 with an increasing amount of MeCP2 and found that the interaction between DGCR8 and Drosha appeared to decrease when MeCP2 level increased (Figure 3C). These results indicate that MeCP2 interaction with DGCR8 suppresses its binding with Drosha. The RNA-binding domains of DGCR8 may be involved in MeCP2 binding, and the essential Drosha-binding C-terminal tail is close to the RNA-binding domains (Yeom et al., 2006). Therefore, the suppressive action of MeCP2 may be caused by a direct competition with Drosha for DGCR8 binding and/or a steric hindrance of MeCP2 on Drosha binding with the DGCR8 C-terminal tail. Together, these results strongly suggest that MeCP2 plays a role in interfering with DGCR8-RNA association, as well as the DGCR8-Drosha interaction, and thereby suppresses DGCR8/Drosha-mediated miRNA processing.

Phosphorylation of MeCP2 at Ser80 Facilitates MeCP2 Binding with DGCR8

Phosphorylation of MeCP2 at Ser80 under resting status is rapidly dephosphorylated upon neuronal activity (Tao et al., 2009; Zhou et al., 2006). Through coIP experiments in HEK293 cells coexpressing DGCR8 and various forms of MeCP2, we found that DGCR8 binding with MeCP2 was significantly lowered when Ser80 of MeCP2 was mutated to phosphorylation-deficient alanine (MeCP2^{S80A}) but elevated when it was mutated to phosphorylation-mimicking aspartate (MeCP2^{S80D}, Figure 3D).

We reproduced a previous finding that MeCP2 is quickly dephosphorylated at the Ser80 site after depolarization (Figure 3E; Tao et al., 2009). To investigate whether the interaction between MeCP2 and DGCR8 may be regulated by neuronal activity, we thus performed a coIP assay with endogenous proteins in primary culture neurons. We found that the interaction of MeCP2

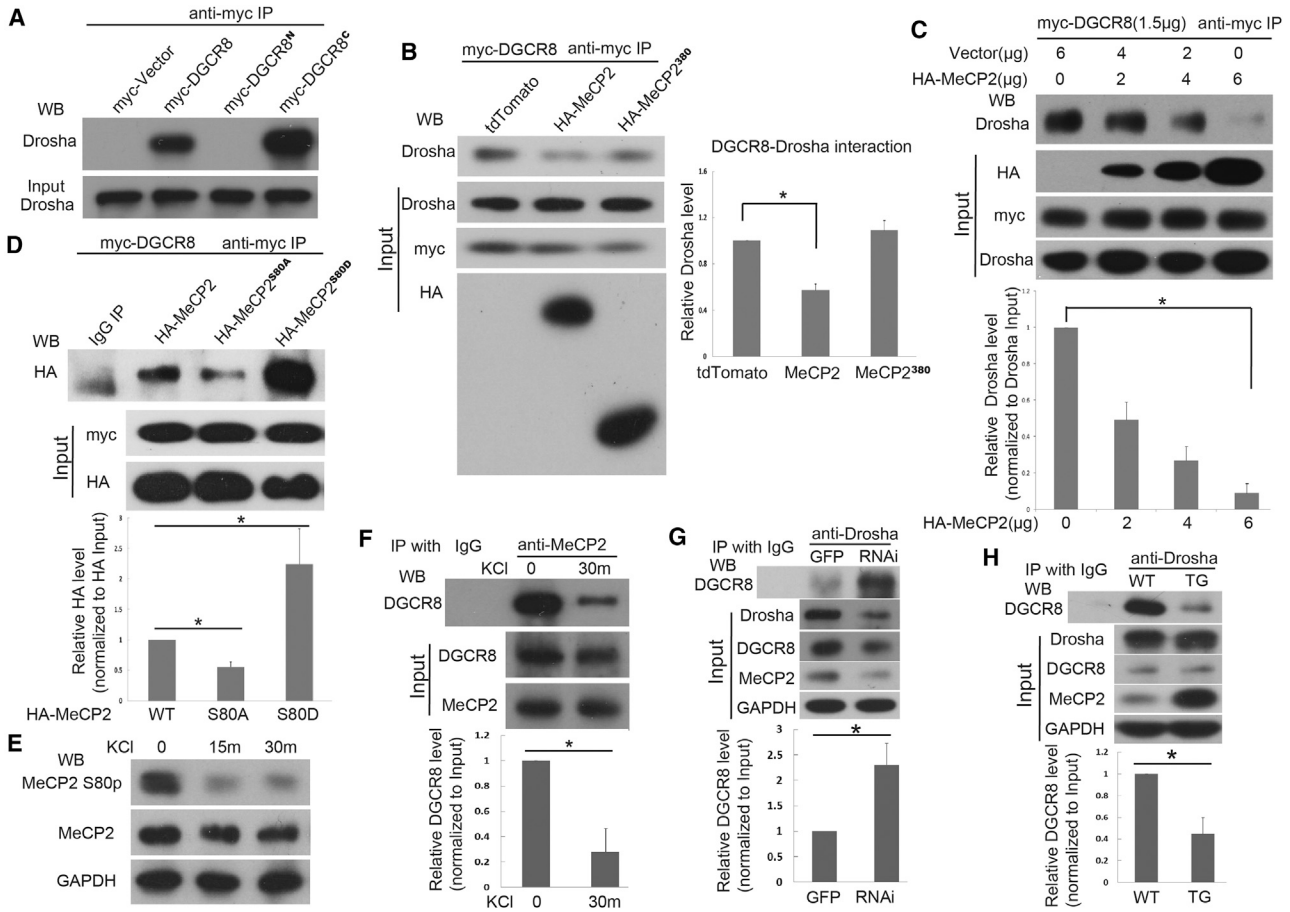

Figure 3. MeCP2 Interrupts the Interaction between DGCR8 and Drosha, Depending on Phosphorylation of Ser80

(A) Drosha binds to the C terminus of DGCR8. Myc-tagged WT, N segment, or C segment of DGCR8 was expressed in 293T cells. Cell lysates were immunoprecipitated with anti-myc antibody and analyzed on SDS-PAGE with Drosha western blotting.

(B) The interaction between Drosha and DGCR8 with the presence of WT MeCP2 and MeCP2^{380}. Myc-tagged DGCR8 was coexpressed with HA-tagged WT MeCP2 or MeCP2^{380}, respectively. Cell lysates were immunoprecipitated with anti-myc antibody and analyzed on SDS-PAGE. Lower panel shows quantification of (B).

(C) The interaction between Drosha and DGCR8 with the different amounts of MeCP2 protein. Different amounts of HA-tagged WT MeCP2 were coexpressed with myc-tagged DGCR8 as indicated. Cell lysates were immunoprecipitated with anti-myc antibody and analyzed on SDS-PAGE. Right panel shows quantification of (C).

(D) Phosphorylation of MeCP2 Ser80 is critical for binding with DGCR8. HA-tagged WT MeCP2, MeCP2^{S80A}, or MeCP2^{S80D} was coexpressed with myc-tagged DGCR8. Cell lysates were immunoprecipitated with anti-myc antibody and analyzed on SDS-PAGE with HA antibody. Lower panel shows quantification of (D).

(E) Western blot of MeCP2 Ser80 upon depolarization. Mouse primary cortical neurons were cultured 5–7 DIV and applied with the stimulus indicated. Samples were collected and analyzed with the antibodies indicated.

(F) Immunoprecipitation of endogenous MeCP2 and DGCR8 from lysates of mouse cultured cortical neurons. Mouse primary cortical neurons were cultured at 5 DIV and stimulated by 50 mM KCl for 30 min and immunoprecipitated with anti-MeCP2 antibody; samples were washed and analyzed on SDS-PAGE by western blot with the antibodies indicated. Lower panel shows quantification of (F).

(G) Interaction between Drosha and DGCR8 in neurons depleting MeCP2. Mouse primary cortical neurons were seeded with either GFP or MeCP2-shRNA-expressing lentivirus at 2 DIV and collected for coIP experiments at 7 DIV. Cell lysates were immunoprecipitated with either IgG or anti-Drosha antibodies and analyzed by SDS-PAGE with antibodies indicated. Lower panel shows quantification of (G).

(H) Interaction between Drosha and DGCR8 in brain lysates of *mecp2* TG mice. Hippocampal lysates were collected from *mecp2* TG and WT littermates and immunoprecipitated with either IgG or anti-Drosha antibodies and analyzed by SDS-PAGE with the antibodies indicated. Lower panel shows quantification of (H). Error bars are SEM. *$p < 0.05$ (t test).

with DGCR8 from lysates of cultured mouse cortical neurons decreased significantly after depolarization (Figure 3F).

Next, we investigated whether the interaction of DGCR8 with Drosha would be affected by MeCP2 in neurons. After knocking down MeCP2 by RNAi, we found that the interaction between DGCR8 and Drosha dramatically increased in mouse cortical culture neurons (Figure 3G). Consistently, interaction between DGCR8 and Drosha appeared to significantly decrease in a *mecp2* transgenic (TG) mice model where *mecp2* was strongly overexpressed genetically, compared to WT littermates (Figure 3H; Collins et al., 2004). Thus, this evidence strongly suggests that MeCP2 interferes with the assembly of the

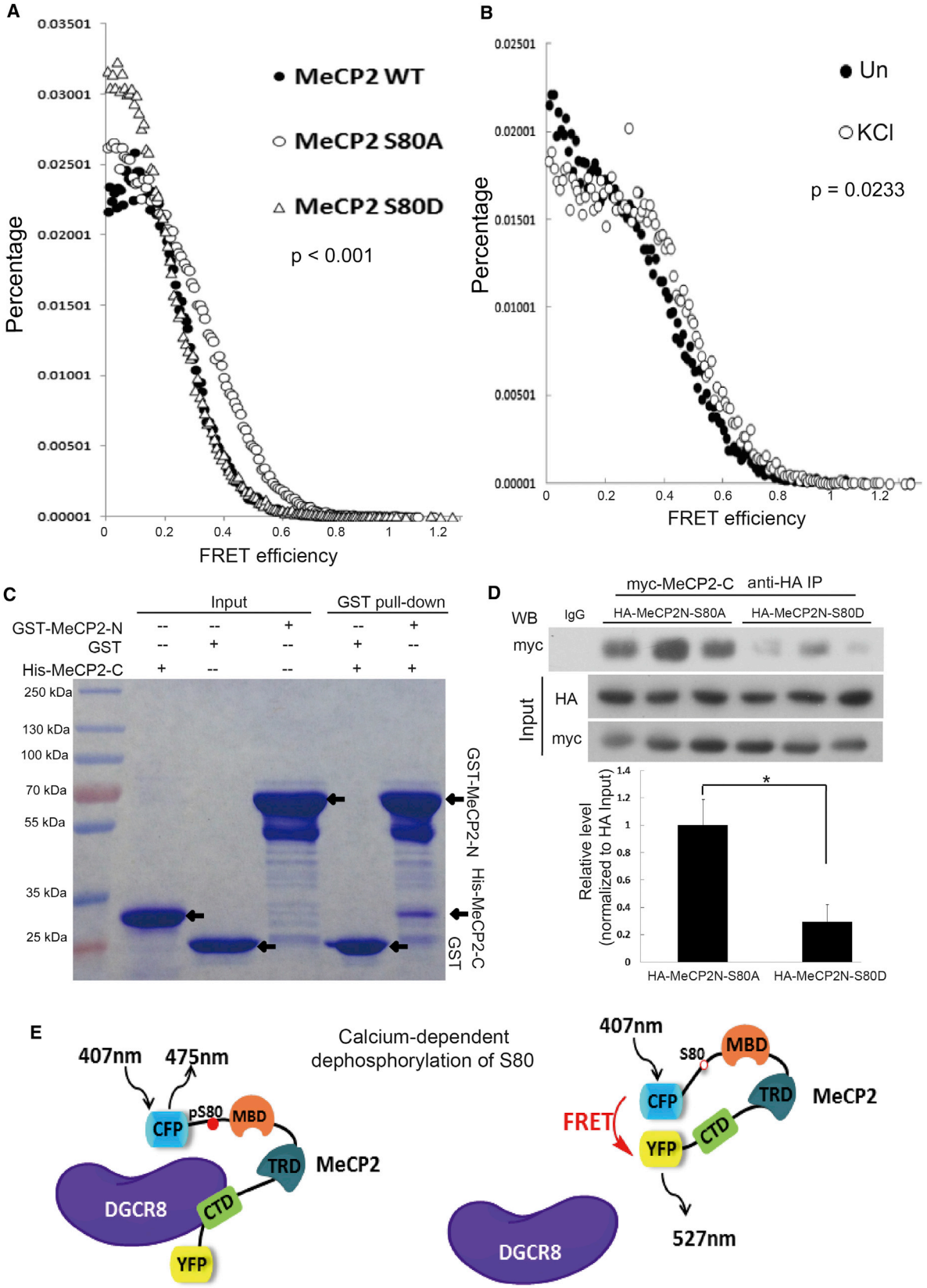

(legend on next page)

DGCR8-Drosha complex and therefore plays a negative role in miRNA processing in vivo.

Intramolecular Interaction of MeCP2 Protein Regulated by the Phosphorylation Status of Ser80

However, as we showed, the N-terminal region of MeCP2 is not required for binding with DGCR8. To address how phosphorylation of Ser80 contributes to the interaction between MeCP2 and DGCR8, we used fluorescence resonance energy transfer (FRET)-based analysis to examine whether phosphorylation of Ser80 would alter the conformation of MeCP2, instead of directly interacting with DGCR8 (Hillebrand et al., 2007). We tagged two distinct fluorescent proteins, cyan fluorescent protein (CFP) and yellow fluorescent protein (YFP), onto the N and C terminus of MeCP2, respectively. The CFP-MeCP2-YFP probe expressed strictly in the nucleus of both 293T cells and mouse primary cortical neurons, as shown by our immunostaining results (Figure S4D). We found that the FRET signals increased when the Ser80 was mutated to phosphorylation-deficient alanine, compared to WT and the MeCP2^{S80D} mutant, because Ser80 of WT MeCP2 is phosphorylated in basal condition in 293T cells (Figures 4B and S4E). These data suggest that there may be intramolecular interactions between the N- and C-terminal halves of unphosphorylated MeCP2, which restrict the accessibility of MeCP2 by DGCR8, and that phosphorylation of Ser80 of MeCP2 opens up the conformation and facilitates its binding to DGCR8, as schematically shown in Figure 4E. We further performed the FRET experiments with the CFP-MeCP2-YFP probe in neurons with and without depolarization stimulus. We found that FRET efficiency of the CFP-MeCP2-YFP probe was increased upon potassium chloride (KCl) stimulus (Figure 4B), supporting that there is a conformational change in MeCP2 protein upon neuronal activity.

To examine this potential intramolecular interaction further, we performed a GST pull-down assay using bacterially purified GST-tagged N (residues 1–305) and His$_6$-tagged C (residues 306–492) terminal halves of MeCP2. We found that there was a direct interaction between GST-MeCP2-N and His-MeCP2-C (Figure 4C). Furthermore, we examined the role of Ser80 phosphorylation in the interaction between MeCP2-N and MeCP2-C using a coIP assay in 293T cells. We found that phosphorylation-deficient MeCP2-N-S80A binds to MeCP2-C in a much stronger fashion, compared to phosphorylation-mimicking MeCP2-N-S80D (Figure 4D). These data indicate that, in the Ser80 unphosphorylated state, MeCP2 forms an intramolecular interaction between its N- and C-terminal halves, which makes the C-terminal half inaccessible for binding to DGCR8.

Taken together, we propose that phosphorylated MeCP2 binds to DGCR8 under resting status in neurons. When neuronal calcium signaling is activated, dephosphorylation of MeCP2 Ser80 leads to its release from DGCR8 and allows activity-dependent miRNA processing to take place (Figure 4E).

MeCP2 Regulates CREB, LIMK1, and Pumilio2 Protein Levels via Suppressing miR-134

To further determine the role of phosphorylation of MeCP2 Ser80 in miRNA processing, we focused on the miR-134, a critical miRNA for neural development (Schratt et al., 2006; Gao et al., 2010). We measured primary, precursor, and mature forms of miR-134 under different manipulations of MeCP2. First, we found that the precursor and mature forms of miR-134, but not primary transcript, were significantly decreased in neurons expressing WT MeCP2, whereas overexpression of the truncated form MeCP2^{380} has no effects on miR-134 levels (Figure 5A).

Consistently, we found that overexpression of phosphorylation-mimicking MeCP2^{S80D} significantly decreased precursor and mature miR-134, but MeCP2^{S80A} has no effect (Figures 5B and 5C). Thus, both our loss- and gain-of-function data indicate that phosphorylation of MeCP2 Ser80 is required for repressing miR-134 processing.

To investigate the functional consequences of MeCP2 regulation of miR-134 processing, we further examined whether the level of targeted proteins of MeCP2-suppressed miR-134 is altered in the absence of MeCP2. It was reported that miR-134 targets three critical regulators for neural development and plasticity: CREB, LIMK1, and Pumilio2 (Fiore et al., 2009; Gao et al., 2010; Schratt et al., 2006). We found that overexpression of MeCP2 in mouse primary cortical neurons indeed leads to an increase of CREB level (Figure 5D). Interestingly, when we coexpressed DGCR8 along with MeCP2 in cortical neurons, we found that the introduction of DGCR8 could neutralize the effect of MeCP2 overexpression and rescue the CREB to the normal level (Figure 5D), suggesting that MeCP2-induced CREB upregulation depends on interaction of MeCP2 and DGCR8. Consistently, we found that the level of mature miR-134 was indeed repressed by MeCP2 overexpression and rescued by coexpression of DGCR8 (Figure 5E). Furthermore, we found that the expression of the MeCP2^{380}-truncated form was not able to increase CREB level

Figure 4. Intramolecular Interactions in MeCP2 Protein Regulated by Phosphorylation of Ser80

(A) FRET efficiency is increased in S80A mutant compared with the WT MeCP2 and MeCP2^{S80D}. CFP and YFP are tagged onto N and C termini of WT MeCP2, MeCP2^{S80A}, and MeCP2^{S80D}. Fluorescence dot signals from ten cells of each condition were collected and measured. $p < 0.001$ (Kolmogorov-Smirnov test).

(B) FRET efficiency is increased in MeCP2 FRET probe upon depolarization in neurons. CFP and YFP are tagged onto N and C termini of WT MeCP2 and are transfected into mouse primary cortical neurons. Under depolarization conditions, neurons were stimulated with 50 mM KCl for 3 hr. Fluorescence signals from ten cells of each condition were collected and measured. $p = 0.023$ (Kolmogorov-Smirnov test).

(C) Direct interaction between GST-MeCP2-N (aa 1–305) and His-MeCP2-C (aa 306–492) shown by GST pull-down assay. The recombinant GST and GST-MeCP2-N purified from bacterial sources were immobilized on glutathione beads, combined with purified His-MeCP2-C, washed, and analyzed on SDS-PAGE.

(D) The interaction between MeCP2-N and MeCP2-C regulated by phosphorylation of Ser80. HA-MeCP2-N-S80A or HA-MeCP2-N-S80D was coexpressed with myc-MeCP2-C. Cell lysates were immunoprecipitated with anti-HA antibody and analyzed on SDS-PAGE. Lower panel shows quantification of (D). Error bars are SEM. *$p < 0.05$ (t test).

(E) In the unphosphorylated state (or the S80A mutant), the accessibility of the MeCP2 C-terminal domain (CTD) is restricted by a potential intramolecular interaction, between the MeCP2 CTD and the MeCP2 N-terminal region including S80. Phosphorylation of S80 increases the CTD accessibility, likely by disrupting this intramolecular inhibition of MeCP2 and forming an open conformation.

See also Figure S4.

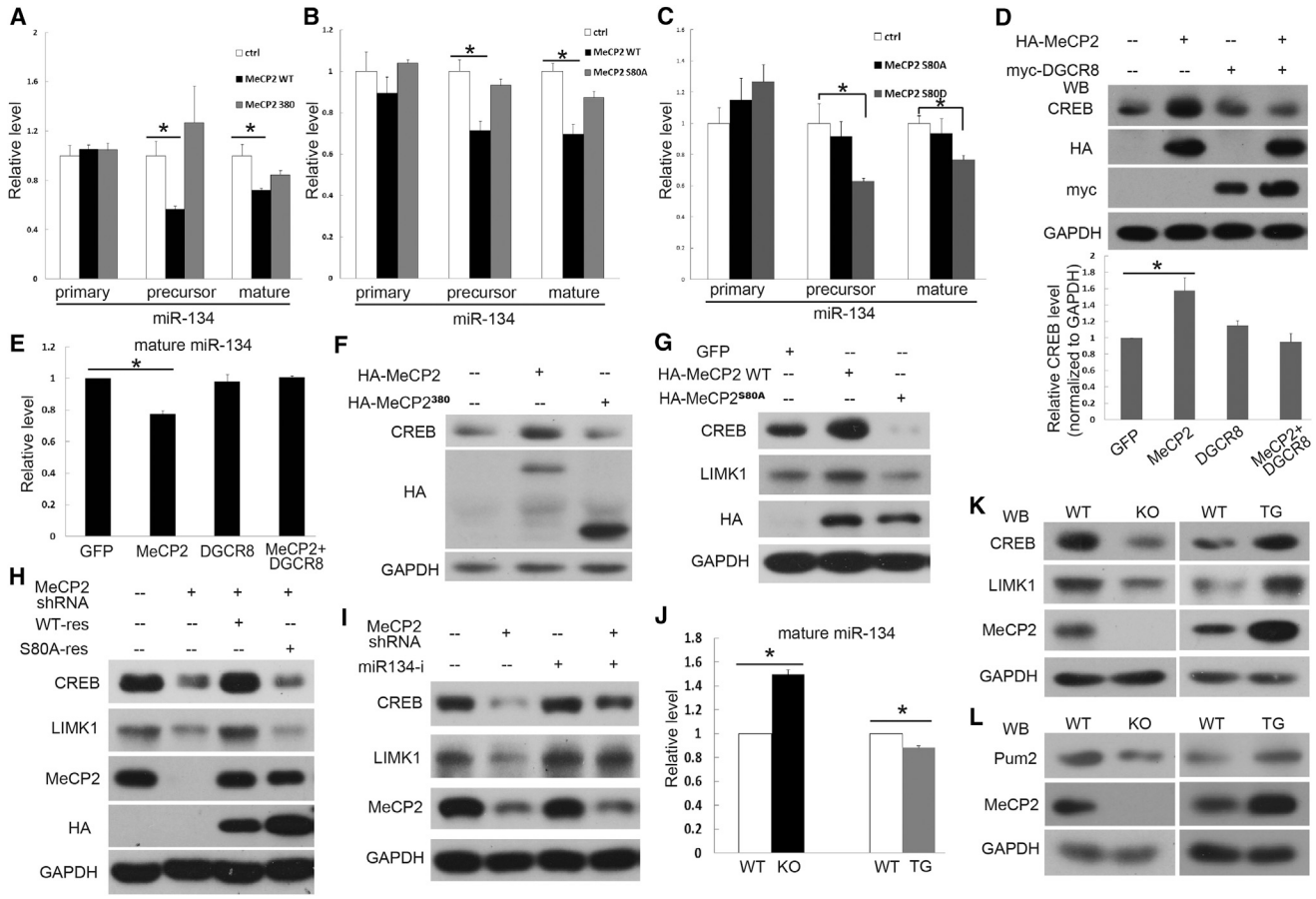

Figure 5. Regulation of CREB, LIMK1, and Pumilio2 Expression by MeCP2 via Suppressing miR-134

(A) Examination of primary, precursor, and mature miR-134 levels in WT and MeCP2^{380} mutation forms of MeCP2-expressing neuron lysates. Lentivirus-harboring WT and 380 truncated forms of MeCP2 were seeded to mouse primary cortical neurons 2 DIV, and RNA samples were collected 5 days after viral infection. Primary, precursor, and mature miR-134 levels were analyzed with qPCR.

(B and C) Examination of primary, precursor, and mature miR-134 levels in WT, S80A, and S80D mutation forms of MeCP2-expressing neuron lysates. The experimental procedure is the same as that in (A).

(D and E) Effect of DGCR8 on MeCP2-regulated levels of miR-134 and CREB. MeCP2- and DGCR8-expressing plasmids were electroporated into mouse primary cortical neurons as indicated. RNA and protein samples were collected 5 days after electroporation. CREB levels were analyzed with western blots. Lower panel shows quantification of (D). (E) miR-134 levels were analyzed with qPCR.

(F) Regulation of CREB level by WT and MeCP2^{380} mutant. Mouse E15 cortical neurons were dissociated and electroporated with GFP, WT, and 380 truncated forms of MeCP2. Cells were lysated at 5–6 DIV and analyzed on SDS-PAGE.

(G) Regulation of CREB and LIMK1 protein level by MeCP2 overexpression. Mouse E15 cortical neurons were dissociated and electroporated with GFP, WT, and S80A mutant forms of MeCP2. Cells were lysated at 5–6 DIV and analyzed on SDS-PAGE.

(H) WT, but not S80A, MeCP2 is able to rescue CREB and LIMK1 protein levels after MeCP2 knockdown. Mouse E15 cortical neurons were dissociated and seeded with lentivirus-harboring shRNA or with shRNA-resistant rescue from WT or S80A form of MeCP2 for 5 days.

(I) miR-134 is required for MeCP2-regulated CREB and LIMK1 expression. Mouse cortical neurons were dissociated and electroporated with miRNA inhibitor control or miR134 inhibitor. Lentivirus-harboring GFP and shRNA against MeCP2 were seed at 2 DIV. Neurons were lysated at 7 DIV and analyzed on SDS-PAGE.

(J) Bidirectional regulation of miR-134 in *mecp2* KO and TG mice. RNAs were collected from hippocampal lysates of *mecp2* KO, TG mice along with their WT littermates. Levels of mature miR-134 were analyzed by qPCR. Error bars are SEM. *$p < 0.05$ (t test).

(K) Bidirectional regulation of CREB and LIMK1 protein levels in *mecp2* KO and TG mice. Left panel shows that CREB and LIMK1 protein levels decreased in hippocampus of *mecp2* KO mice. Hippocampal samples were collected from 2-week-old *mecp2* KO mice and WT littermates. Right panel shows that CREB and LIMK1 protein levels were elevated in hippocampus of *mecp2* TG mice. Hippocampal samples were collected from 2-week-old *mecp2* TG and WT littermates.

(L) Bidirectional regulation of Pumilio2 protein levels in *mecp2* KO and TG mice. Left panel shows that Pum2 protein levels decreased in hippocampus of *mecp2* KO mice. Hippocampal samples were collected from 2-week-old WT and KO mice. Right panel shows that Pum2 protein levels were elevated in hippocampus of *mecp2* TG mice. Hippocampal samples were collected from 2-week-old WT and *mecp2* TG mice.

See also Figures S5 and S6.

in cortical neurons as WT MeCP2 (Figure 5F). These data indicate that the interaction with DGCR8 is critical for MeCP2 to posttranscriptionally regulate CREB level.

We found that the CREB and LIMK1 protein levels were significantly elevated when the WT MeCP2, but not MeCP2^{S80A}, was overexpressed in cultured neurons, consistent with our finding

that MeCP2^{S80A} showed much weaker interaction with DGCR8 than WT MeCP2 (Figure 5G). Next, we found that the expression of WT MeCP2 with same-sense mutations of shRNA-targeting sites in these neurons rescued the reduction of CREB and LIMK1 caused by MeCP2 RNAi, whereas the expression of MeCP2^{S80A} also containing same-sense mutations had no effect on CREB and LIMK1 protein levels (Figure 5H). These data indicate that the phosphorylation of the MeCP2 S80 site is essential for upregulation of CREB level by MeCP2 overexpression, further suggesting that interfering with miRNA processing by MeCP2 could lead to multiple physiological consequences by affecting target gene expression.

Importantly, we found that the protein levels of CREB and LIMK1 were also decreased by downregulating MeCP2 with expression of specific shRNA in cultured cortical neurons, which was largely blocked by introducing the miR-134 inhibitor that was complementary to the mature miR-134 (Figure 5I), strongly suggesting that miR-134 is required for MeCP2 regulating CREB and LIMK1 protein levels. Notably, the levels of primary miR-134 transcripts, CREB, and LIMK1 remain constant under these manipulations, indicating that the regulation by MeCP2 on these components occurs at the posttranscriptional level (Figures S5A–S5F).

We also examined the protein level of Pumilio2 under different manipulations of MeCP2. Consistently, we found that Pumilio2 protein level decreases in MeCP2 RNAi and increases in MeCP2 overexpression samples (Figure S5G). The mRNA levels of Pumilio2 are not altered in either MeCP2 RNAi or overexpression conditions, compared to control (Figure S5H).

To determine whether miR-134 and its target proteins would be regulated in vivo, we examined levels of mature miR-134, CREB, LIMK1, and Pumillio2 proteins in hippocampal lysates of MeCP2 KO and TG mice, using WT littermates as control (Chen et al., 2001; Collins et al., 2004). First, we found that the mature miR-134 level significantly increased in brain lysates of *mecp2* KO, whereas it decreased in those of *mecp2* TG, compared to WT mice (Figure 5J). Next, we found that the level of CREB and LIMK1 dramatically decreased in the hippocampus of *mecp2* KO mice as compared to WT (left panel of Figure 5K). On the other hand, we found that CREB and LIMK1 protein levels notably increased in *mecp2* TG mice (right panel of Figure 5K). This is consistent with the previous finding that the protein level of CREB was increased in the hypothalamus of *mecp2* TG mice compared to WT mice (Chahrour et al., 2008). Importantly, mRNA levels of primary miR-134, CREB, and LIMK1 were not affected in either *mecp2* KO or TG mice (Figures S6A–S6F). We also found that the protein level of Pumilio2 decreased in the hippocampus of *mecp2* KO and increased in the hippocampus of *mecp2* TG mouse (Figure 5L). Taken together, these data indicate that MeCP2 posttranscriptionally controls levels of miR-134, CREB, LIMK, and Pumilio2 protein in vivo.

Repression of Dendritic Growth by MeCP2 via Controlling miRNA Processing

Next, we would like to address how the interaction of MeCP2 with DGCR8 contributes to neural development. The duplications of *MECP2*-containing loci lead to severe autism spectrum disorders in human, suggesting that gain-of-function mutations of *MECP2* may cause destructive consequences to the development of the nervous system (Ramocki et al., 2009). Consistently, it was reported that dendritic growth of hippocampal neurons is inhibited when MeCP2 is elevated and TG mouse with *mecp2* overexpression appears to have phenotypes mimicking the *MECP2* duplication disorders (Zhou et al., 2006). Furthermore, CREB, LIMK1, and Pumilio2, these target genes of MeCP2 shown above, were reported to play critical roles in regulating dendritic growth (Redmond et al., 2002; Schratt et al., 2006; Vessey et al., 2010).

We would like to address whether this inhibition of dendritic growth by MeCP2 is due to the repression of miR-134. We examined the dendritic growth of the mouse primary cortical culture neurons and found that expression of WT MeCP2, not MeCP2^{S80A} and MeCP2^{380}, leads to strong inhibition of dendritic growth (Figures 6A and 6B). We coexpressed miR-134 and its antisense control along with WT MeCP2 in cultured neurons. Strikingly, we found that expression of miR-134 was able to fully rescue the dendritic growth defects caused by WT MeCP2 overexpression, but miR-134 antisense control had no effect (Figures 6A and 6B). We expressed miR-134 and the MeCP2 RNAi construct alone in the cortical neurons and found that there were no significant changes in dendritic growth (Figures S7A–S7D). These data indicate that MeCP2 represses neuronal dendritic growth by suppressing miR-134.

Next, we asked whether the calcium-dependent dephosphorylation of MeCP2 Ser80 may contribute to the well-characterized activity-dependent dendritic growth process in neurons (Redmond et al., 2002). We transfected WT MeCP2 and MeCP2^{S80D} mutation into mouse primary cortical neurons and depolarized the neuron with KCl. We found that the activity-dependent dendritic growth was completely abolished only when the S80D mutated form of MeCP2 was introduced, indicating that calcium-dependent dephosphorylation of MeCP2 Ser80 is required for activity-dependent dendritic outgrowth (Figures 6C and 6D).

Finally, we examined the role of MeCP2 in dendritic growth and spine development in hippocampal slice culture preparations. We used gene gun-based DNA delivery on rat postnatal day 7 (P7) hippocampal slice cultures and found that introduction of WT MeCP2 significantly decreased dendritic growth, as measured by total dendritic length (Figures 7A and 7B). However, overexpression of two mutant forms of MeCP2, MeCP2^{S80A} and MeCP2^{380}, had no such effect (Figures 7A and 7B). Note that MeCP2^{S80A} and MeCP2^{380} are not able to bind to DGCR8 and repress miRNA processing. Furthermore, we measured spine density in the above preparations and found that overexpression of WT MeCP2, but not MeCP2^{S80A} and MeCP2^{380}, strongly repressed spine density in hippocampal slice culture, further suggesting that the role of MeCP2 on spine development also requires the interaction of MeCP2 and DGCR8 (Figures 7C and 7D; Han et al., 2013; Schratt et al., 2006). Taken together, these results indicate that the gain of function of MeCP2 leads to inhibition of dendritic and spine growth, depending on the repression of DGCR8/Drosha-dependent miR-134 processing by MeCP2.

DISCUSSION

In this study, we have identified a mechanism by which MeCP2 regulates gene expression by suppressing nuclear miRNA

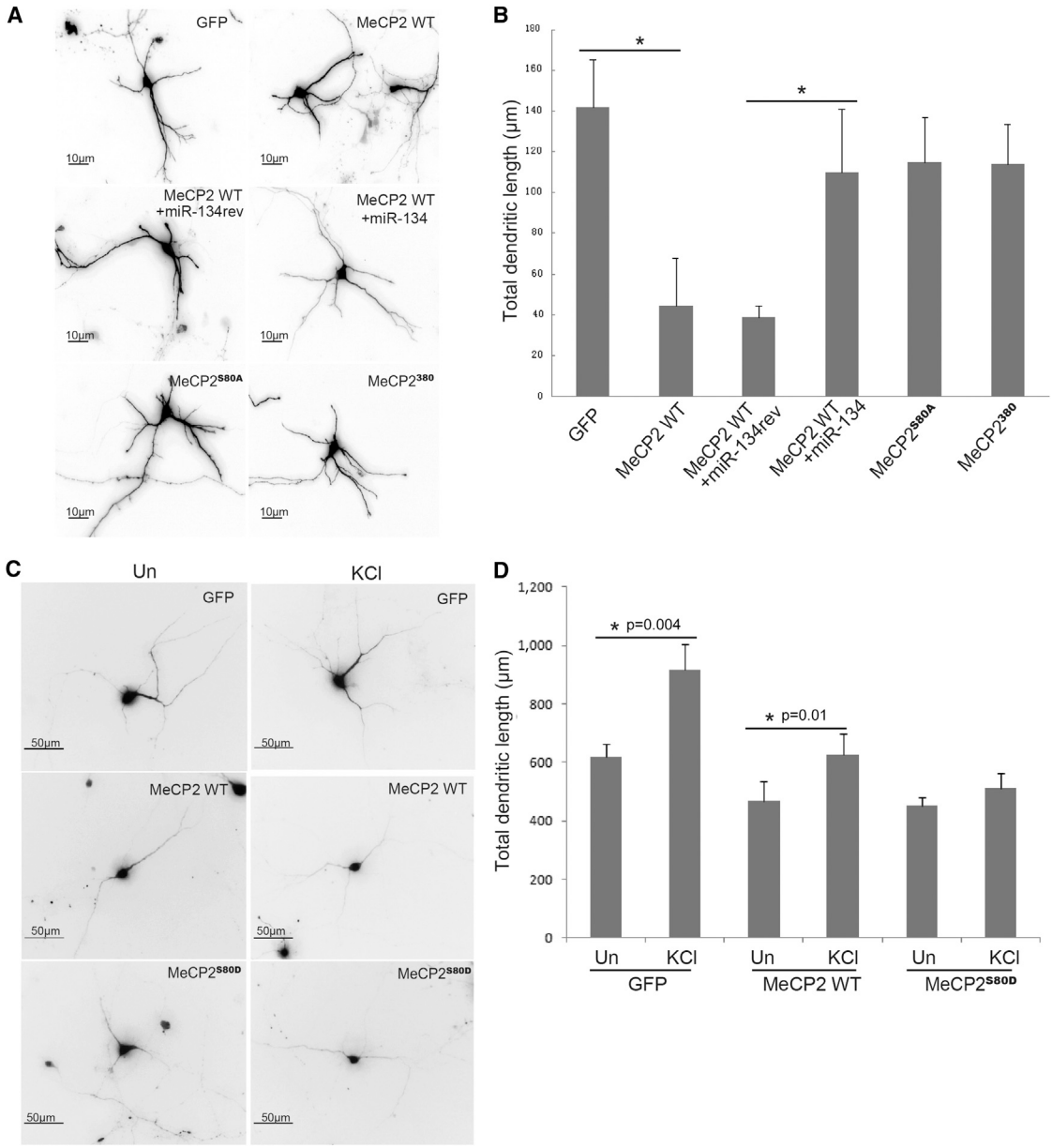

Figure 6. MeCP2 Regulates Dendritic Growth by Inhibiting miR-134, and Dephosphorylation of MeCP2 S80 Is Required for Activity-Dependent Dendritic Growth

(A) Example picture of mouse primary cortical neurons transfected at 3 DIV with GFP alone and GFP with constructs indicated. Neurons were fixed and immunostained with GFP antibody at 6 DIV for measurement of dendritic length.

(B) Measurements of total dendritic length of each condition. *$p < 0.01$ (t test).

(C) Example picture of mouse primary cortical neurons with each construct transfected. Constructs expressing MeCP2 WT and mutations were transfected into cortical neuron 2 DIV and stimulated by KCl 48 hr after transfection. KCl with a final concentration of 25 mM was given to mouse primary cortical neurons for 36 hr before neurons were fixed and performed following experiments. Immunostaining with GFP antibody was used to examine the dendritic growth.

(D) Measurements of total dendritic length of each condition. *$p < 0.01$ (t test). A total 12–15 neurons from each condition were randomly selected and measured. See also Figure S7.

processing through direct interaction with DGCR8, a key component of the processing complex. This mechanism could contribute significantly to the MeCP2's regulation of proteins that play important neuronal functions, e.g., CREB, LIMK1, and Pumilio2.

Here, we showed that as a nuclear protein, MeCP2 could not only repress gene transcription by binding to methylated DNA and recruiting transcriptional repressors (Nan et al., 1998) but also suppress miRNA processing by binding to RNA-binding domains of DGCR8. Whether MeCP2 may interact with other RNA-binding proteins and participate in RNA biogenesis and metabolism needs to be further investigated. The previous study that MeCP2 interacts with the RNA-splicing complex suggests

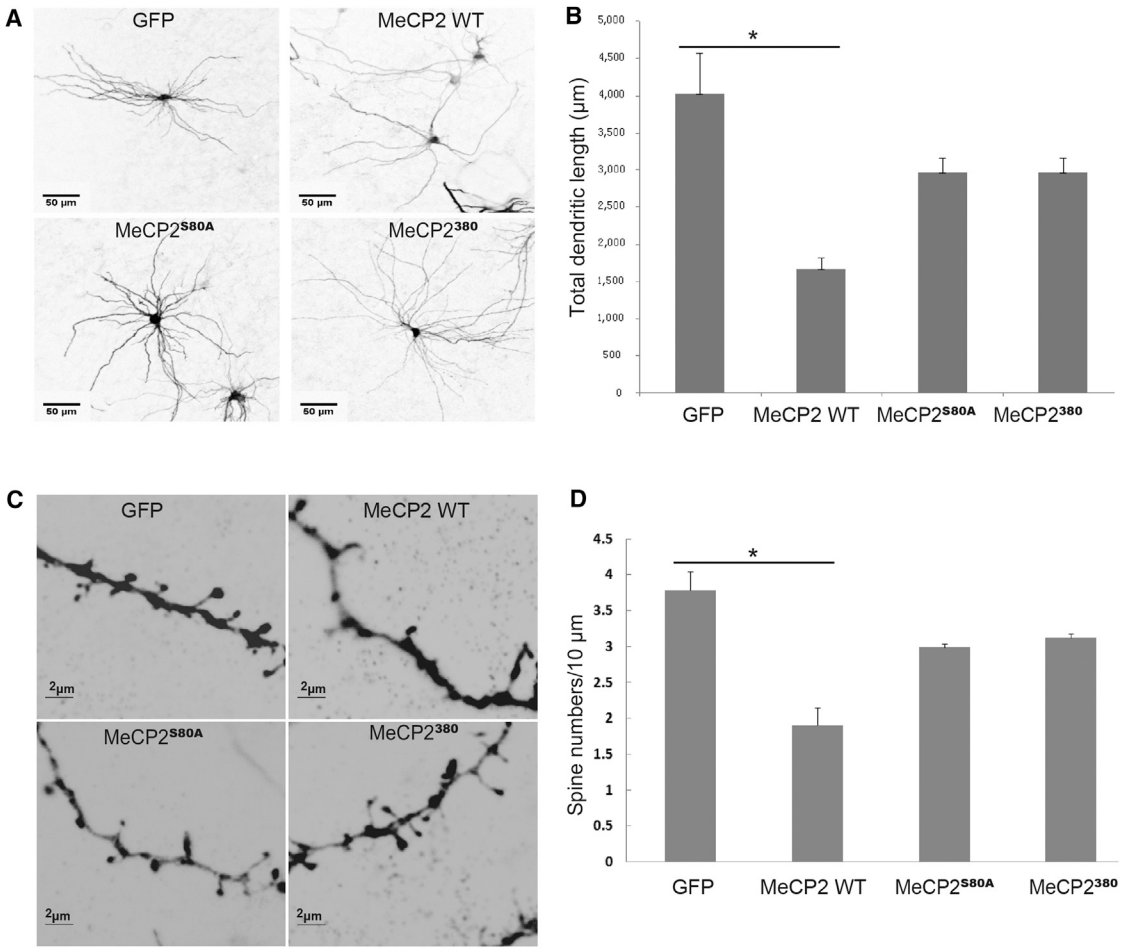

Figure 7. MeCP2 Inhibits Dendritic Growth and Spine Formation in Hippocampal Slice Cultures

(A) Typical pictures of rat hippocampal slice culture neurons. Hippocampal slices from P7 rat were transfected at 3 DIV with GFP alone and GFP with MeCP2, MeCP2^{S80A}, and MeCP2^{380} by gene gun delivery. Slices were fixed and immunostained with GFP antibody at 9 DIV.

(B) Measurements of total dendritic length of each condition. *$p < 0.01$ (t test). For each condition, 18 neurons were randomly selected and measured. At least 900 μm dendrites were analyzed for each condition.

(C) Typical pictures of spines of rat hippocampal slice culture neurons. Experimental procedures are the same as (A).

(D) Measurements of spine density over 10 μm dendrites of each condition. *$p < 0.01$ (t test).

that MeCP2 may be widely involved in RNA metabolism processes (Young et al., 2005).

How miRNA biogenesis in neurons is regulated by neuronal activity is an important question. A previous report showed that light-induced neuronal activity is critical for fast turnover of mature miRNAs in retina cells (Krol et al., 2010). Our study suggests that miRNA biogenesis may be positively regulated by neural activity, as controlled by calcium-dependent dephosphorylation of MeCP2 and derepressing of miRNA processing. Thus, this work may represent regulation over different levels or in different tissues. We suggest that MeCP2-regulated nuclear miRNA processing plays a critical role for miRNA biogenesis in cortical and hippocampal neurons.

It is important that nuclear miRNA processing is critical for proper synaptic function as shown by Ullian and colleagues that deletion of DGCR8 leads to defects of inhibitory synaptic transmission (Hsu et al., 2012). Whether MeCP2 may be involved in inhibitory synaptic transmission via controlling nuclear miRNA processing would be an interesting question to address.

An important issue regarding the pathophysiology of MeCP2-related disorders is that both loss and gain of functions of MeCP2 lead to severe pathological symptoms. Loss-of-function mutations of *MECP2* lead to RTT, whereas duplication of *MECP2*-containing locus leads to autism spectrum disorders. It is difficult to provide a satisfactory explanation for why a higher level of this protein leads to diseases, if solely considering the transcriptional regulation point of view. Our study showed that MeCP2 could regulate expression levels of target genes by fine-tuning the level of miRNAs, as shown for CREB, LIMK1, and Pumilio2 protein levels. Thus, this mechanism provides an alternative explanation for the dose effect of MeCP2 in neural development. As we showed in the Results, increasing the amount of MeCP2 protein leads to repression of mature miR-134, which then causes various dysregulation of protein targets as well as cellular consequences.

Nuclear miRNA processing is a highly regulated process, as exemplified by the effects of p53 and SMAD proteins that are involved in tumorigenesis (Davis et al., 2008; Suzuki et al., 2009). Our finding of a posttranscriptional function of MeCP2 in regulating miRNA maturation suggests that intervening dysregulated miRNA processing represents a potential therapeutic approach in the treatment of RTT.

EXPERIMENTAL PROCEDURES

Plasmids

The rat MeCP2-e2 gene was a gift of Dr. Adrian Bird. Other constructs of MeCP2 mutations and truncations were all generated based on this construct. In brief, MeCP2^{S80D}, MeCP2$^{\Delta MBD}$, MeCP2^{S80A}, and MeCP2^{380} were generated using KOD-Plus (Toyobo) according to manufacturer's instructions. The mouse MeCP2 shRNA was directed against the sequence as follows: 5′-AAGTCA GAAGACCAGGATC-3′. MeCP2 siRNAs (Thermo Scientific, against mouse MeCP2, on-target plus SMART pool L-044034-09-12, 5′-CCUGAAGGUUGG ACACGAA-3′, 5′-UGACAAAGCUUCCCGAUUA-3′, 5′-CCGAAUUGCUGCUG CUUUA-3′, and 5′-CGAAAUGGCUGUGUAGCAA-3′), along with scrambled siRNA as control. miR-134 sequence was amplified with primers as the following: forward, 5′-cagtgaattcccaaccttggtgaggcagctg-3′; and reverse, 5′-cagtgaattctcctggtccactgagcaggc-3′. The miR-134 sequence or reverse and complement sequence was inserted into FUGW to get miR-134 plasmid/miR-134rev plasmid. mmu-miR-134 inhibitor was purchased from GenePharma.com. Inhibitors are 2-methylated-modified RNA oligo completely complementary to mmu-miR-134 and purified by high-performance liquid chromatography prior to being used. miR-134 inhibitors were introduced into neurons by Amaxa Nucleofector at the time of seeding. The mouse *DGCR8* cDNA was amplified from total cDNA of mouse cortical neurons. DGCR8 truncations were generated as described previously by Yeom et al. (2006).

Antibodies

Antibodies used in this study were as follows: MeCP2 (#3456, Cell Signaling Technology; MP4591, MP4601, ECM Biosciences); Drosha (#3364; Cell Signaling Technology); DGCR8 (sc-48473; Santa Cruz Biotechnology); Myc epitope tag (#M20002; Abmart); HA epitope tag (#M20013; Abmart); GST (#2622; Cell Signaling Technology); CREB (#9197; Cell Signaling Technology); LIMK1 (#3842; Cell Signaling Technology); and GAPDH (ab8245; Abcam).

Cell Culture

Embryonic day 15 (E15)–E16 mouse cortical cells were cultured and transfected with Amaxa Nucleofector in 6-well plates. Cells were collected at 5–7 days in vitro (DIV) for further analysis. Lentivirus used in this study was made with 10^8–10^9 viral genome/ml by the Obio Technology (Shanghai) and the Neuronbiotech.

Genetic-Modified Mice

mecp2 TG mice (008679) and nestin-cre mice (003771) were purchased from Jackson Laboratory; *mecp2* null (000415) and loxP-floxed *mecp2* (011918) were purchased from Mutant Mouse Regional Resource Center at University of California Davis. The use and care of animals complied with the guideline of the Animal Advisory Committee at the Shanghai Institutes for Biological Science, CAS.

Quantitative Real-Time PCR Assays

For quantitative real-time PCR assays, total RNA was extracted from mouse cortical neurons using *mirVana* miRNA Isolation Kit (Ambion). For the measurement of primary miRNA transcripts, the large-sized RNA fractions (>200 bp) were used for reverse transcription. cDNA was synthesized by poly-dT primers from 1 μg of purified RNA (>200 bp fraction) by iScript cDNA Synthesis Kit (Bio-Rad). SYBR Premix Ex Taq from Takara was used in this study. Quantitative real-time PCR was performed with the Rotor-Gene Q machine (QIAGEN). Results were normalized to GAPDH, and data analysis was done by using the comparative C_T method in software by QIAGEN.

For the measurement of precursor and mature miRNA levels, small fraction RNAs (<200 bp) were isolated with *mirVana* miRNA Isolation Kit. Mature miRNAs were detected and quantified with Hairpin-it miRNAs qPCR Quantification Kit (GenePharma). For the measurement of precursor miRNAs, small RNA fraction was reverse transcribed with miScript II RT Kit (QIAGEN) and quantified with quantitative real-time PCR assays using precursor-specific primers from QIAGEN.

Primers used in quantitative real-time PCR assays were as follows:
miR-134 forward, 5′-GGGTGTGTGACTGGTTGACCA-3′
miR-134 reverse, 5′-GGGTTGGTGACTAGGTGGCC-3′
CREB forward, 5′-TCAGCCGGGTACTACCATTC-3′
CREB reverse, 5′-TTCAGCAGGCTGTGTAGGAA-3′
LIMK1 forward, 5′-ATGAGGTTGACGCTACTTTGTTG-3′
LIMK1 reverse, 5′-CTACACTCGCAGCACCTGAA-3′
miR-383 forward, 5′-CTCCTCAGATCAGAAGGTGACTG-3′
miR-383 reverse, 5′-CTCTTTCTGACCAGGCAGTG-3′
miR-382 forward, 5′-TTGAAGAGAAGTTGTTCGTGGTG-3′
miR-382 reverse, 5′-GTGTTGTCCGTGAATGATTCGT-3′
miR-182 forward, 5′-CCATTTTTGGCAATGGTAGAAC-3′
miR-182 reverse, 5′-CATAGTTGGCAAGTCTAGAACC-3′
miR-137 forward, 5′-ACTCTCTTCGGTGACGGGTA-3′
miR-137 reverse, 5′-CGCTGGTACTCTCCTCGACT-3′
miR-132 forward, 5′-ACCGTGGCTTTCGATTGTTA-3′
miR-132 reverse, 5′-GGCGACCATGGCTGTAGACT-3′
miR-128 forward, 5′-ATTGGCCTTCTTCCTGAGC-3′
miR-128 reverse, 5′-TCAGGAAGCAGCTGAAAAAG-3′
miR-7a forward, 5′-TGGATGTTGGCCTAGTTCTG-3′
miR-7a reverse, 5′-TGGCAGACTGTGATTTGTTG-3′
let-7i forward, 5′-CCCTGGCTGAGGTAGTAGTTTG-3′
let-7i reverse, 5′-ATCACCAGCACTAGCAAGGC-3′
miR-27b forward, 5′-TGCAGAGCTTAGCTGATTGG-3′
miR-27b reverse, 5′-CCTTCTCTTCAGGTGCAGAAC-3′
miR-27a forward, 5′-GAGGAGCAGGGCTTAGCTG-3′
miR-27a reverse, 5′-CAGGGGGCGGAACTTAGC-3′
miR-124-1 forward, 5′-TGTTCACAGCGGACCTTGA-3′
miR-124-1 reverse, 5′-GAAGCCTGCTACCCGTACT-3′
miR-124-2 forward, 5′-TGCAATGAGTCACTTGCTTC-3′
miR-124-2 reverse,: 5′- CCCTTCCTAACTTCTCTCGG-3′
miR-124-3 forward, 5′-AGCGGACCTTGATTTAATGTC-3′
miR-124-3 reverse, 5′-GGGCCATTTCCATGAGAAAG-3′
miR-153 forward, 5′-CGGTGTCATTTTTGTGACGT-3′
miR-153 reverse, 5′-CAATGATCACTTTTGTGACTATGC-3′
miR-135a forward, 5′-AAGTGACTCACCTCTGCCAG-3′
miR-135a reverse, 5′-TGCCAGCATTTCAGTGTGTG-3′
miR-340 forward, 5′-CTTGGTGTGATTATAAAGCAATGA-3′
miR-340 reverse, 5′-CCAGGTATGGCTATAAAGTAACTGA-3′
BDNF forward, 5′-TGCCTAGATCAAATGGAGCTTCTC-3′
BDNF reverse, 5′-CCGATATGTACTCCTGTTCTTCAGC-3′
PUM2, forward 5′-TCCTCATCCAGTTTGCATTTAG-3′
PUM2, reverse 5′-TCAGATCTATTATAGCGGAGCC-3′.

GST Pull-Down Assay

GST pull-down assay was performed as described before (Qiu and Ghosh, 2008). Overnight express TB medium from Novagen (catalog #71491-4) was used to generate recombinant protein from *E. coli*.

Immunoprecipitation

For coIP in 293T cells, HEK293T cells were cultured on 6-well plates, and transfection was performed when the cells reached 50% confluence. FuGENE HD (Roche, Promega) was used for transfection. A total of 5 μg of DNA was used per well in 6-well plates at a molar ratio of 1:1 for myc-tagged and HA-tagged constructs. Cells were harvested 24 hr after transfection. The cells were rinsed with ice-cold PBS, harvested, and lysed for 20 min at 4°C in a modified RIPA buffer. Of the supernatant, 5% was saved for the input control, and the rest was incubated with 2 μg anti-HA agarose beads (Abmart) or anti-myc agarose beads overnight at 4°C. The immune complex was washed three times with the lysis buffer, then boiled in 1× SDS loading buffer with 20 mM DTT, and resolved by the 10% SDS-PAGE. The gel was transferred to polyvinylidene fluoride membranes (Amersham), and the membrane was blocked with 5% milk in Tris-buffered saline and Tween 20 (TBST) buffer for 1 hr. It

was then incubated overnight at 4°C with primary antibodies, washed three times in TBST, and the signals were revealed by horseradish peroxidase reaction using the SuperSignal Chemiluminescent Substrate (Pierce).

RNA-Seq Deep Sequencing

Hippocampus RNA samples were prepared from P30 WT and KO mice and were sequenced and analyzed by Solexa of BGI Shenzhen. RNA-seq sample preparation and data analysis were performed as described by Kwak et al. (2009). RNA from cultured mouse cortical neurons with MeCP2 manipulations and depolarization stimulus were collected 5–7 DIV and sequenced by Solexa GAII of Shanghai Bio-Chip. Standard Solexa TruSeq-Small RNA sequence protocol was used. The technical method is described in the TruSeq Small RNA Sample preparation guide on the Illumina website. CLC Genomics Workbench V5.5 was used to perform miRNA data analysis. RNA-seq data analysis was performed by Novel Bioinformatics.

FRET Assay

FRET assays were performed as described by Hillebrand et al. (2007) with modifications. 293 cells were transfected with CFP-MeCP2, MeCP2-YFP, CFP-MeCP2-YFP, and CFP-MeCP2^{80A}-YFP and fixed after 48 hr. Primary cultured cortical neurons were transfected in the same way and stimulated with KCl for 3 hr before fixation. All quantified FRET data were collected using a Nikon A1 laser scan confocal microscope with Plan Apo VC 60× Oil DIC N2. CFP was excited using 457 nm laser lines, and emission was collected for donor (482 nm) and FRET (540 nm) simultaneously, whereas YFP was excited using 514 nm laser lines, and emission was collected at 540 nm. For each treatment, ten cells were analyzed, and more than 2,000 signals per cell were calculated. FRET signal was corrected by YFP and CFP bleed-through emissions. FRET ratio was calculated with Fiji software using the emission sensitize method.

$$\frac{\text{FRET } a \times \text{CFP } b \times \text{YFP}}{\sqrt{\text{CFP} \times \text{YFP}}}$$

Alpha-Binding Assay

The measurement was based on the "Determining Kd with an Alpha assay" protocol from PerkinElmer. Glutathione donor beads and Ni-chelate acceptor beads (PerkinElmer) were used in this assay. GST-tagged mouse DGCR8 (aa 483–773) and His-tagged rat MeCP2 (aa 170–492) were overexpressed in *E. coli* and purified by affinity column and HiTrap SP cation exchange column. Gradients of untagged mouse DGCR8 (aa 483–773) (4.5 nM–45 μM) were used to titrate the interaction between GST-tagged DGCR8 (aa 483–773) and His-tagged MeCP2 (aa 170–492). The concentrations of GST-DGCR8 (aa 483–773) and His-MeCP2 (aa 170–492) used were 25 and 2.5 nM, respectively. The concentration for both donor and acceptor beads was 10 μg ml^{-1}. The assay was done in a solution containing 1× PBS buffer (pH 7.4), 0.2% (w/v) BSA, 1 mM DTT, and 0.03% (v/v) Tween 20. Data were analyzed with a one-site competition model using nonlinear regression with GraphPad Prism software.

Dendritic Length Analysis

The length of dendritic branches in primary cultured cortical neurons was determined as the following: EGFP-positive neurons were selected randomly from each condition, and the total length of all protrusions was analyzed using Neurolucida software (MBF Bioscience). All quantifications were tested with a Student's t test and expressed as SEM. Results were considered significant if $p < 0.05$. At least three independent experiments were performed, and 10–18 neurons per transfection condition were analyzed.

Hippocampus Slice Culture and Immunostaining

The 350 μm hippocampus slices were prepared using P7 rats and cultured as described in Zhou et al. (2006). Slices were cultured on Millicell (0.4 μm; Millipore) in 6-well dishes containing 750 μl of medium and incubated in 5% CO_2 at 37°C. Transfection was performed with a Helios Gene Gun (Bio-Rad) at 3 DIV. Bullets were prepared using plasmids containing 75 μg DNA and were coated on 25 mg 1.0 μm gold particles (Bio-Rad). Slices were fixed at 9 DIV in 4% paraformaldehyde, and GFP immunostaining was performed using anti-GFP (Invitrogen) and Alexa 488-conjugated secondary antibody (1:1,000). Slices were also stained with DAPI (1:1,000) to visualize cell nuclei.

Slice Imaging and Analysis

Images were acquired with a Zeiss LSM5 510 laser-scanning confocal microscope. Images across experiments were acquired with identical settings. Eight-bit images were obtained using a 20× objective at 1,024 × 1,024 pixel resolution. Images were acquired as a z stack with about 13–15 sections (1 μm/section). Dendritic length was analyzed with Fiji software.

Spine Density Analysis

For spine density analysis, confocal z stacks of neurons in hippocampal slices were acquired with LSM510 Laser Scanning Confocal microscope, using an oil-immersion 60× objective lens. Images were analyzed with Fiji software. Protrusions in direct contact with the dendrites were counted as spines, and the average spine density was calculated as the number of spines per 10 μm dendritic length. At least 900 μm dendrites from seven or more neurons were analyzed for each condition.

SUPPLEMENTAL INFORMATION

Supplemental Information includes seven figures and one table and can be found with this article online at http://dx.doi.org/10.1016/j.devcel.2014.01.032.

ACKNOWLEDGMENTS

We thank Dr. Mu-ming Poo for his critical comments on the manuscript. We thank Dr. Adrian Bird for providing rat MeCP2 cDNA. This work was supported by the 973 Program Grant 2011CBA00400, CAS Hundreds of Talents Program, Strategic Priority Research Program of the Chinese Academy of Science Grant XDB02050400 to Z.Q.

Received: August 12, 2013
Revised: January 1, 2014
Accepted: January 31, 2014
Published: March 10, 2014

REFERENCES

Amir, R.E., Van den Veyver, I.B., Wan, M., Tran, C.Q., Francke, U., and Zoghbi, H.Y. (1999). Rett syndrome is caused by mutations in X-linked MECP2, encoding methyl-CpG-binding protein 2. Nat. Genet. *23*, 185–188.

Bartel, D.P. (2004). MicroRNAs: genomics, biogenesis, mechanism, and function. Cell *116*, 281–297.

Bebbington, A., Percy, A., Christodoulou, J., Ravine, D., Ho, G., Jacoby, P., Anderson, A., Pineda, M., Ben Zeev, B., Bahi-Buisson, N., et al. (2010). Updating the profile of C-terminal MECP2 deletions in Rett syndrome. J. Med. Genet. *47*, 242–248.

Buschdorf, J.P., and Strätling, W.H. (2004). A WW domain binding region in methyl-CpG-binding protein MeCP2: impact on Rett syndrome. J. Mol. Med. *82*, 135–143.

Bushati, N., and Cohen, S.M. (2007). microRNA functions. Annu. Rev. Cell Dev. Biol. *23*, 175–205.

Chahrour, M., and Zoghbi, H.Y. (2007). The story of Rett syndrome: from clinic to neurobiology. Neuron *56*, 422–437.

Chahrour, M., Jung, S.Y., Shaw, C., Zhou, X., Wong, S.T., Qin, J., and Zoghbi, H.Y. (2008). MeCP2, a key contributor to neurological disease, activates and represses transcription. Science *320*, 1224–1229.

Chen, R.Z., Akbarian, S., Tudor, M., and Jaenisch, R. (2001). Deficiency of methyl-CpG binding protein-2 in CNS neurons results in a Rett-like phenotype in mice. Nat. Genet. *27*, 327–331.

Chen, W.G., Chang, Q., Lin, Y., Meissner, A., West, A.E., Griffith, E.C., Jaenisch, R., and Greenberg, M.E. (2003). Derepression of BDNF transcription involves calcium-dependent phosphorylation of MeCP2. Science *302*, 885–889.

Cohen, S., Gabel, H.W., Hemberg, M., Hutchinson, A.N., Sadacca, L.A., Ebert, D.H., Harmin, D.A., Greenberg, R.S., Verdine, V.K., Zhou, Z., et al. (2011). Genome-wide activity-dependent MeCP2 phosphorylation regulates nervous system development and function. Neuron *72*, 72–85.

Collins, A.L., Levenson, J.M., Vilaythong, A.P., Richman, R., Armstrong, D.L., Noebels, J.L., Sweatt, D.J., and Zoghbi, H.Y. (2004). Mild overexpression of MeCP2 causes a progressive neurological disorder in mice. Hum. Mol. Genet. *13*, 2679–2689.

Davis, B.N., Hilyard, A.C., Lagna, G., and Hata, A. (2008). SMAD proteins control DROSHA-mediated microRNA maturation. Nature *454*, 56–61.

Denli, A.M., Tops, B.B., Plasterk, R.H., Ketting, R.F., and Hannon, G.J. (2004). Processing of primary microRNAs by the Microprocessor complex. Nature *432*, 231–235.

Ebert, D.H., Gabel, H.W., Robinson, N.D., Kastan, N.R., Hu, L.S., Cohen, S., Navarro, A.J., Lyst, M.J., Ekiert, R., Bird, A.P., and Greenberg, M.E. (2013). Activity-dependent phosphorylation of MeCP2 threonine 308 regulates interaction with NCoR. Nature *499*, 341–345.

Fiore, R., Khudayberdiev, S., Christensen, M., Siegel, G., Flavell, S.W., Kim, T.K., Greenberg, M.E., and Schratt, G. (2009). Mef2-mediated transcription of the miR379-410 cluster regulates activity-dependent dendritogenesis by fine-tuning Pumilio2 protein levels. EMBO J. *28*, 697–710.

Fire, A., Xu, S., Montgomery, M.K., Kostas, S.A., Driver, S.E., and Mello, C.C. (1998). Potent and specific genetic interference by double-stranded RNA in *Caenorhabditis elegans*. Nature *391*, 806–811.

Gao, J., Wang, W.Y., Mao, Y.W., Gräff, J., Guan, J.S., Pan, L., Mak, G., Kim, D., Su, S.C., and Tsai, L.H. (2010). A novel pathway regulates memory and plasticity via SIRT1 and miR-134. Nature *466*, 1105–1109.

Gregory, R.I., Yan, K.P., Amuthan, G., Chendrimada, T., Doratotaj, B., Cooch, N., and Shiekhattar, R. (2004). The Microprocessor complex mediates the genesis of microRNAs. Nature *432*, 235–240.

Guy, J., Cheval, H., Selfridge, J., and Bird, A. (2011). The role of MeCP2 in the brain. Annu. Rev. Cell Dev. Biol. *27*, 631–652.

Han, J., Lee, Y., Yeom, K.H., Kim, Y.K., Jin, H., and Kim, V.N. (2004). The Drosha-DGCR8 complex in primary microRNA processing. Genes Dev. *18*, 3016–3027.

Han, K., Gennarino, V.A., Lee, Y., Pang, K., Hashimoto-Torii, K., Choufani, S., Raju, C.S., Oldham, M.C., Weksberg, R., Rakic, P., et al. (2013). Human-specific regulation of MeCP2 levels in fetal brains by microRNA miR-483-5p. Genes Dev. *27*, 485–490.

Hillebrand, M., Verrier, S.E., Ohlenbusch, A., Schäfer, A., Söling, H.D., Wouters, F.S., and Gärtner, J. (2007). Live cell FRET microscopy: homo- and heterodimerization of two human peroxisomal ABC transporters, the adrenoleukodystrophy protein (ALDP, ABCD1) and PMP70 (ABCD3). J. Biol. Chem. *282*, 26997–27005.

Hsu, R., Schofield, C.M., Dela Cruz, C.G., Jones-Davis, D.M., Blelloch, R., and Ullian, E.M. (2012). Loss of microRNAs in pyramidal neurons leads to specific changes in inhibitory synaptic transmission in the prefrontal cortex. Mol. Cell. Neurosci. *50*, 283–292.

Krol, J., Busskamp, V., Markiewicz, I., Stadler, M.B., Ribi, S., Richter, J., Duebel, J., Bicker, S., Fehling, H.J., Schübeler, D., et al. (2010). Characterizing light-regulated retinal microRNAs reveals rapid turnover as a common property of neuronal microRNAs. Cell *141*, 618–631.

Kwak, P.B., Wang, Q.Q., Chen, X.S., Qiu, C.X., and Yang, Z.M. (2009). Enrichment of a set of microRNAs during the cotton fiber development. BMC Genomics *10*, 457.

Lee, Y., Ahn, C., Han, J., Choi, H., Kim, J., Yim, J., Lee, J., Provost, P., Rådmark, O., Kim, S., and Kim, V.N. (2003). The nuclear RNase III Drosha initiates microRNA processing. Nature *425*, 415–419.

Lewis, J.D., Meehan, R.R., Henzel, W.J., Maurer-Fogy, I., Jeppesen, P., Klein, F., and Bird, A. (1992). Purification, sequence, and cellular localization of a novel chromosomal protein that binds to methylated DNA. Cell *69*, 905–914.

Lyst, M.J., Ekiert, R., Ebert, D.H., Merusi, C., Nowak, J., Selfridge, J., Guy, J., Kastan, N.R., Robinson, N.D., de Lima Alves, F., et al. (2013). Rett syndrome mutations abolish the interaction of MeCP2 with the NCoR/SMRT co-repressor. Nat. Neurosci. *16*, 898–902.

Martinowich, K., Hattori, D., Wu, H., Fouse, S., He, F., Hu, Y., Fan, G., and Sun, Y.E. (2003). DNA methylation-related chromatin remodeling in activity-dependent BDNF gene regulation. Science *302*, 890–893.

Nan, X.S., Meehan, R.R., and Bird, A. (1993). Dissection of the methyl-CpG binding domain from the chromosomal protein MeCP2. Nucleic Acids Res. *21*, 4886–4892.

Nan, X.S., Ng, H.H., Johnson, C.A., Laherty, C.D., Turner, B.M., Eisenman, R.N., and Bird, A. (1998). Transcriptional repression by the methyl-CpG-binding protein MeCP2 involves a histone deacetylase complex. Nature *393*, 386–389.

Qiu, Z., and Ghosh, A. (2008). A calcium-dependent switch in a CREST-BRG1 complex regulates activity-dependent gene expression. Neuron *60*, 775–787.

Qiu, Z., Sylwestrak, E.L., Lieberman, D.N., Zhang, Y., Liu, X.Y., and Ghosh, A. (2012). The Rett syndrome protein MeCP2 regulates synaptic scaling. J. Neurosci. *32*, 989–994.

Ramocki, M.B., Peters, S.U., Tavyev, Y.J., Zhang, F., Carvalho, C.M., Schaaf, C.P., Richman, R., Fang, P., Glaze, D.G., Lupski, J.R., and Zoghbi, H.Y. (2009). Autism and other neuropsychiatric symptoms are prevalent in individuals with MeCP2 duplication syndrome. Ann. Neurol. *66*, 771–782.

Redmond, L., Kashani, A.H., and Ghosh, A. (2002). Calcium regulation of dendritic growth via CaM kinase IV and CREB-mediated transcription. Neuron *34*, 999–1010.

Schratt, G.M., Tuebing, F., Nigh, E.A., Kane, C.G., Sabatini, M.E., Kiebler, M., and Greenberg, M.E. (2006). A brain-specific microRNA regulates dendritic spine development. Nature *439*, 283–289.

Suzuki, H.I., Yamagata, K., Sugimoto, K., Iwamoto, T., Kato, S., and Miyazono, K. (2009). Modulation of microRNA processing by p53. Nature *460*, 529–533.

Szulwach, K.E., Li, X.K., Smrt, R.D., Li, Y.J., Luo, Y.P., Lin, L., Santistevan, N.J., Li, W.D., Zhao, X.Y., and Jin, P. (2010). Cross talk between microRNA and epigenetic regulation in adult neurogenesis. J. Cell Biol. *189*, 127–141.

Tao, J.F., Hu, K.P., Chang, Q., Wu, H., Sherman, N.E., Martinowich, K., Klose, R.J., Schanen, C., Jaenisch, R., Wang, W.D., and Sun, Y.E. (2009). Phosphorylation of MeCP2 at Serine 80 regulates its chromatin association and neurological function. Proc. Natl. Acad. Sci. USA *106*, 4882–4887.

Urdinguio, R.G., Fernandez, A.F., Lopez-Nieva, P., Rossi, S., Huertas, D., Kulis, M., Liu, C.G., Croce, C.M., Calin, G.A., and Esteller, M. (2010). Disrupted microRNA expression caused by Mecp2 loss in a mouse model of Rett syndrome. Epigenetics *5*, 656–663.

Vessey, J.P., Schoderboeck, L., Gingl, E., Luzi, E., Riefler, J., Di Leva, F., Karra, D., Thomas, S., Kiebler, M.A., and Macchi, P. (2010). Mammalian Pumilio 2 regulates dendrite morphogenesis and synaptic function. Proc. Natl. Acad. Sci. USA *107*, 3222–3227.

Wu, H., Tao, J., Chen, P.J., Shahab, A., Ge, W., Hart, R.P., Ruan, X., Ruan, Y., and Sun, Y.E. (2010). Genome-wide analysis reveals methyl-CpG-binding protein 2-dependent regulation of microRNAs in a mouse model of Rett syndrome. Proc. Natl. Acad. Sci. USA *107*, 18161–18166.

Yeom, K.H., Lee, Y., Han, J., Suh, M.R., and Kim, V.N. (2006). Characterization of DGCR8/Pasha, the essential cofactor for Drosha in primary miRNA processing. Nucleic Acids Res. *34*, 4622–4629.

Young, J.I., Hong, E.P., Castle, J.C., Crespo-Barreto, J., Bowman, A.B., Rose, M.F., Kang, D., Richman, R., Johnson, J.M., Berget, S., and Zoghbi, H.Y. (2005). Regulation of RNA splicing by the methylation-dependent transcriptional repressor methyl-CpG binding protein 2. Proc. Natl. Acad. Sci. USA *102*, 17551–17558.

Zhou, Z., Hong, E.J., Cohen, S., Zhao, W.N., Ho, H.Y., Schmidt, L., Chen, W.G., Lin, Y., Savner, E., Griffith, E.C., et al. (2006). Brain-specific phosphorylation of MeCP2 regulates activity-dependent Bdnf transcription, dendritic growth, and spine maturation. Neuron *52*, 255–269.